Integrated diagnostic evaluation of multiple malignant neoplasms via ^{99m}Tc-MDP three-phase bone imaging: A case report

JING-YI LIAN, JIAN-LIN LU, HUI-YU ZHENG, SI-XIA YUAN and JIN-SHAN ZHANG

Department of Nuclear Medicine, The Third Affiliated Hospital of Guangzhou Medical University, Guangzhou, Guangdong 510150, P.R. China

Received April 23, 2025; Accepted September 25, 2025

DOI: 10.3892/ol.2025.15412

Abstract. Multiple primary malignant neoplasms (MPMNs) are two or more independent cancer types arising in different organs, either at the same time or one after another. Diagnosing MPMNs is often difficult as multiple organs can be involved and early symptoms may be subtle or absent. The present study reports the case of a 79-year-old man with a recurrent left forearm mass whose ^{99m}Tc-labeled methylene diphosphonate (^{99m}Tc-MDP) three-phase bone scan unexpectedly showed a classic 'superscan'. Surgical pathology confirmed two primary malignancies: Subcutaneous myxofibrosarcoma and prostate cancer with extensive bone metastases. The present case illustrates how ^{99m}Tc-MDP imaging, especially when combined with single photon emission computed tomography/computed tomography, can reveal both soft-tissue tumors and diffuse skeletal involvement, thereby improving early detection of MPMNs.

Correspondence to: Professor Jin-Shan Zhang, Department of Nuclear Medicine, The Third Affiliated Hospital of Guangzhou Medical University, 63 Duobao Road, Guangzhou, Guangdong 510150, P.R. China
E-mail: gysy_nuclemed@163.com

Abbreviations: CT, computed tomography; ^{18}F-FDG, ^{18}F-fluorodeoxyglucose; IARC/IACR, International Agency for Research on Cancer/International Association of Cancer Registries; LHRH, luteinizing hormone releasing hormone; MFS, myxofibrosarcoma; MMPMN, metachronous multiple primary malignant neoplasm; MPMN, multiple primary malignant neoplasm; MRI, magnetic resonance imaging; PET, positron emission tomography; PSA, prostate-specific antigen; PSMA, prostate-specific membrane antigen; SEER, Surveillance Epidemiology and End Results; SMPMN, synchronous multiple primary malignant neoplasm; SPECT, single photon emission computed tomography; ^{99m}Tc-MDP, ^{99m}Tc-labeled methylene diphosphonate

Key words: ^{99m}Tc-MDP three-phase bone imaging, multiple primary malignant neoplasms, myxofibrosarcoma, super bone imaging, case report

Introduction

Multiple primary malignant neoplasms (MPMNs) are defined as the presence of two or more histologically distinct primary cancer types arising in separate organs or anatomical sites in the same patient (1-4). Although the reported incidence of MPMNs in China remains low (ranging from 0.4 to 2.4%) it has steadily increased in recent years owing to advances in imaging and diagnostic methodologies (4-6). The widely accepted diagnostic framework combines the original Warren criteria (1) with the modifications from Liu *et al* (2), which stipulate that: i) Each neoplasm must be confirmed as malignant by histopathology; ii) each neoplasm must display unique pathological features; iii) tumors must develop in non-contiguous locations; and iv) each tumor must demonstrate an independent pattern of metastasis, thereby excluding secondary spread or recurrence. Nevertheless, clinicians frequently encounter challenges in differentiating multiple primary tumors from metastases due to overlapping clinical presentations, limitations of conventional imaging and difficulties in accurately determining tumor origin on pathological examination (7). These factors contribute to increased rates of both misdiagnosis and underdiagnosis.

In the present case report, the case of a 79-year-old male patient diagnosed with multiple primary malignant neoplasms is described. The coexistence of distinct malignancies posed substantial diagnostic challenges, particularly in differentiating primary lesions from potential metastatic disease. The present study highlights the utility of ^{99m}Tc-labeled methylene diphosphonate (^{99m}Tc-MDP) three-phase bone imaging in providing integrated diagnostic information that facilitates accurate evaluation and clinical decision-making.

Case report

Chief complaint. A 79-year-old male patient, who had a forearm lesion present for >5 years with recurrence noted in the past 6 months, was admitted to the Department of Joint Surgery at the Third Affiliated Hospital of Guangzhou Medical University (Guangzhou, China) in March 2024.

History of present illness. The patient first noticed a painless nodular lesion on the left forearm in 2020 without any apparent cause. After local excision, histopathology revealed nodular

fasciitis (Fig. S1). In 2021 (1 years later) the lesion recurred at the same site and grew to 6x4 cm. Despite the notable increase in size, the patient remained asymptomatic and underwent a skin tumor resection at the Department of Joint Surgery, The Third Affiliated Hospital of Guangzhou Medical University. The excised tissue was fixed in 4% neutral phosphate-buffered formaldehyde solution at room temperature (~25˚C) for 24 h. The specimens were sectioned at a thickness of 4 μm and stained using hematoxylin and eosin (H&E) reagents [Roche Diagnostics (Shanghai) Co., Ltd.] at 25˚C for 8 h. The stained slides were examined under a light microscope (Olympus BX43; Olympus Corporation) at x100 magnification, and representative images were captured for histopathological evaluation. Histopathological analysis revealed fibrous tissue proliferation, spindle-shaped tumor cells with nuclear atypia and inflammatory cell infiltration, accompanied by myxoid degeneration, hemorrhage and frequent mitotic figures (4 per high-power field) (Fig. S2). The differential diagnoses included nodular fasciitis and malignant mesenchymal tumor. At this time, the clinical diagnosis was a cutaneous tumor, and no further specific treatment was administered following the excision.

In December 2023 (onset time), the patient noticed two new lesions at the original site, measuring 3x3x2 and 2x2x1 cm. The overlying skin showed erythema and swelling, but no additional symptoms were reported. In March 2024, the patient presented to the Surgical Outpatient Clinic at the Third Affiliated Hospital of Guangzhou Medical University for evaluation. Throughout the course of the illness, the patient maintained normal bowel movements and stable mental status, but experienced urinary frequency and urgency, and occasional hematuria, without significant changes in sleep, appetite or weight.

Past medical and family history. The patient had no history of trauma, fractures, tumors or other relevant medical conditions. The patient had no family history of malignancy, and no history of exposure to carcinogenic chemicals, radiation or toxic substances. The patient also reported no history of smoking, alcohol use or illicit drug use.

Physical examination. On March 26, 2024, a physical examination of the left forearm revealed a 6x4 cm subcutaneous lesion with well-defined borders and an indurated, rubbery consistency. The lesion was partially movable upon palpation and was without any signs of inflammation. Palpation revealed two additional lesions in the left forearm. The larger lesion measured 3x3x2 cm with well-defined borders and the smaller measured 2x2x1 cm with poorly defined borders. A longitudinal surgical scar was noted on the skin surface of the left forearm.

Preoperative laboratory tests. The preoperative laboratory tests revealed the following results: Red blood cell count, 2.88×10^{12}/l (reference range, 4.3-5.8x10^{12}/l); and hemoglobin, 81 g/l (reference range, 130-175 g/l). The white blood cell count, platelet count, coagulation profile and liver and kidney function tests were all within the normal limits.

Preoperative imaging. In April 2024, magnetic resonance imaging (MRI) of the left forearm demonstrated multiple irregular subcutaneous lesions on the dorsal aspect measuring 46x27x60 and 38x12x72 mm. These lesions showed hypointensity on T1-weighted imaging and heterogeneous signal intensity on T2-weighted imaging and proton density-weighted imaging, along with notable heterogeneous enhancement and poorly defined borders on contrast-enhanced imaging (Fig. 1). Despite the indistinct margins, the lesions remained well-demarcated from the adjacent muscles. The osseous structures appeared normal with an intact and continuous cortex. No evidence of destructive bony changes, osseous metastasis or abnormal signal intensity was observed. T1-weighted contrast-enhanced imaging revealed no abnormal bone enhancement (Fig. 1C, F, H and L). Although X-ray, thin-section bone window computed tomography (CT) and 3D-CT were not performed due to financial constraints and clinical priorities, the absence of peri-tumoral bone destruction on MRI definitively excluded direct osseous invasion, strongly suggesting local recurrence of the soft-tissue sarcoma.

Concurrent ^{99m}Tc-MDP three-phase bone imaging revealed markedly increased perfusion to the left forearm following radiotracer injection, along with localized abnormal radiotracer uptake during the blood pool phase, suggesting the possibility of soft tissue pathology (Fig. 2A and B). Whole-body bone imaging demonstrated diffusely increased skeletal radiotracer uptake, with multiple irregularly shaped, heterogeneous foci exhibiting moderate to high intensity in the cervical and thoracolumbar spine, bilateral ribs, pelvis and proximal femurs (Fig. 2C and D). Such imaging results are consistent with widespread bone metastasis, indicating extensive involvement and heterogeneous uptake across the skeletal system. The kidneys exhibited minimal tracer uptake, and the bladder showed limited concentration, resulting in a characteristic 'superscan' pattern (Fig. 2C and D). Single photon emission CT (SPECT)/CT fusion imaging confirmed multiple osteoblastic changes in the thoracolumbar spine, ribs and pelvis, along with soft-tissue lesions in the dorsal left forearm showing reduced ^{99m}Tc-MDP uptake, without evidence of significant bone involvement (Fig. 2C and D). Due to the financial constraints and advanced age of the patient, X-ray, thin-section bone window CT and 3D CT imaging were not performed.

Treatment process and follow-up pathology. Following the ^{99m}Tc-MDP whole-body three-phase bone scan, the left forearm lesion was highly suspected to be malignant, with augmented blood flow and increased bone metabolic activity. Nevertheless, the extensive bone metastases, indicative of multiple secondary lesions, are atypical for fibrosarcoma. In April 2024, a prostate-specific antigen (PSA) test revealed a markedly elevated total PSA level of 563.864 ng/ml (reference range for age >80 years, 0-8 ng/ml), raising a strong suspicion of an underlying malignancy. A subsequent CT scan demonstrated heterogeneous bone density with multiple sclerotic and lytic lesions in the hips and lumbar vertebrae, findings that are highly indicative of metastatic bone disease (Fig. 3A-C). Additionally, significant prostate enlargement was identified (Fig. 3D), which, in conjunction with the elevated PSA levels and the extent of skeletal involvement, provided compelling evidence supporting the diagnosis of advanced prostate cancer. Pathological examination of the pubic bone biopsy confirmed metastatic adenocarcinoma consistent with a prostatic primary origin. The diagnosis of advanced prostate adenocarcinoma had been established previously, as aforementioned.

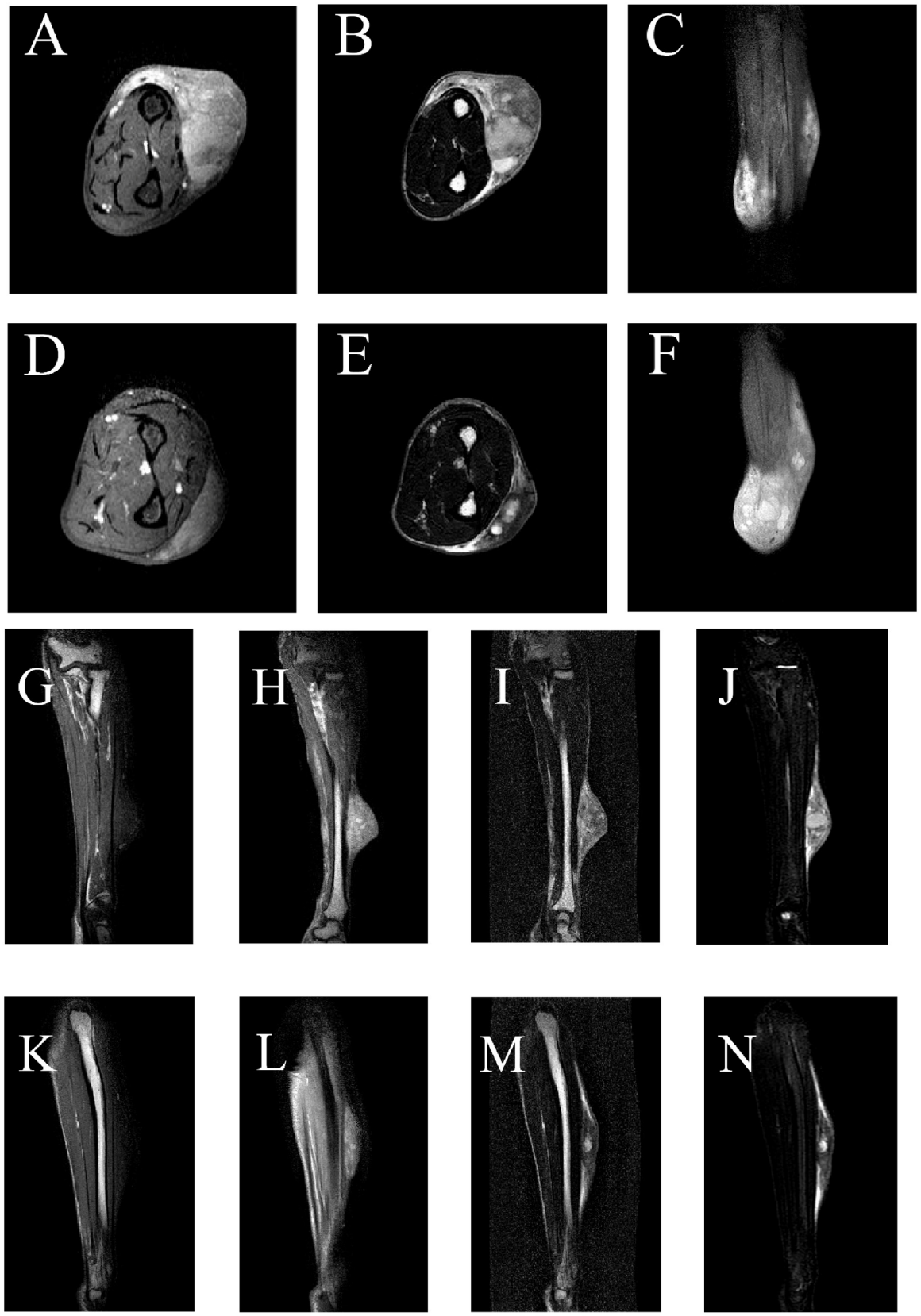

Figure 1. Axial, coronal and sagittal MRI scans of the left forearm with multiple malignant tumors. (A) Axial T1- and (B) T2-weighted images of the larger lesion. (C) Coronal T1-weighted contrast-enhanced image of entire lesion. (D) Axial T1- and (E) Axial T2-weighted images of the smaller lesion. (F) Coronary PDW-weighted image of entire lesion. (G) Sagittal T1-weighted and (H) Sagittal T1-weighted contrast-enhanced images of the larger lesion. (I) Sagittal T2-weighted and (J) Sagittal T2 fat-suppressed images of the larger lesion. (K) Sagittal T1-weighted and (L) Sagittal T1-weighted contrast-enhanced images of the smaller lesion. (M) Sagittal T2-weighted and (N) Sagittal T2 fat-suppressed images of the smaller lesion. The two largest lesions measured 46x27x60 and 38x12x72 mm. The lesions exhibited uneven enhancement in T1-weighted images and displayed heterogeneous iso- and hyperintense signals in T2-weighted images. The PDWI sequences also demonstrated high signal intensity, while contrast-enhanced scans revealed heterogeneous and marked enhancement. MRI demonstrated subcutaneous lesions with heterogeneous enhancement, clearly separated from surrounding muscle tissue. MRI, magnetic resonance imaging; PDWI, proton density-weighted imaging.

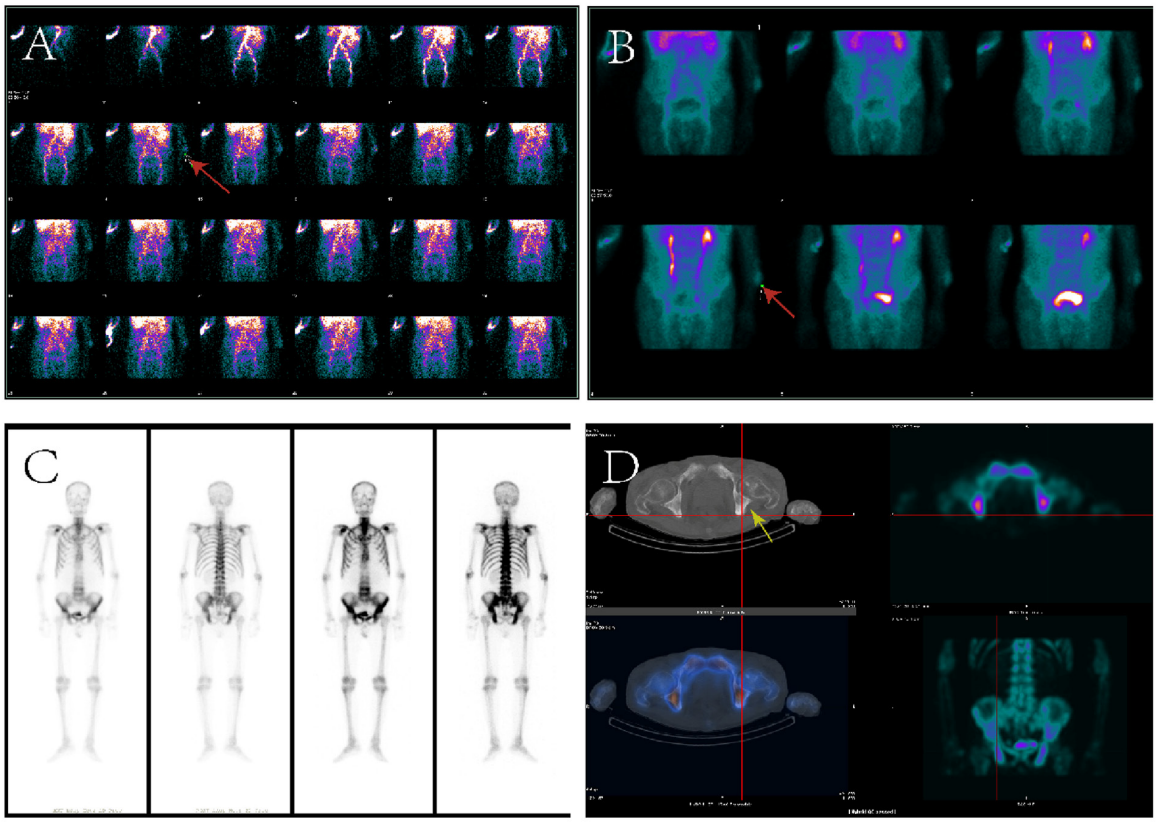

Figure 2. ^{99m}Tc-labeled methylene diphosphonate three-phase bone imaging of the dual primary myxofibrosarcoma involving subcutaneous tissue and prostate cancer with multiple bone metastases. (A) Blood perfusion phase showing the blood flow phase of the left forearm, indicating increased local perfusion (red arrow). (B) Blood pool phase showing the blood pool phase, revealing a focal area of radiotracer accumulation in the left forearm (red arrow). (C) Whole-body three-phase bone imaging demonstrating significantly increased radiotracer uptake across the skeleton, consistent with a 'superscan' appearance. (D) Single photon emission computed tomography/computed tomography fusion image (lumbar, pelvic and forearm regions) in bone window settings, identifying multiple patchy areas of increased bone density (yellow arrow), predominantly indicative of osteoblastic activity.

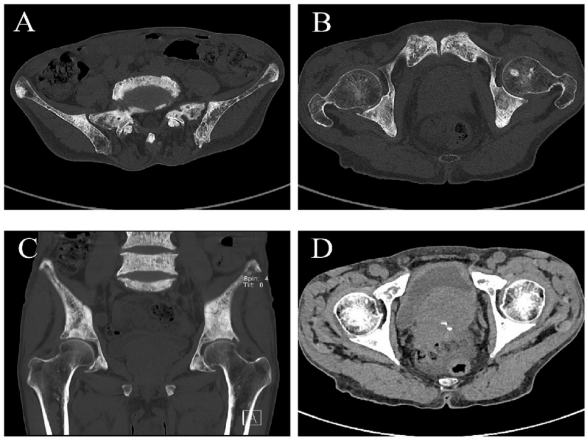

Figure 3. High-resolution thin-section CT of pelvis and prostate. (A) (Bone window) Multiple areas of osteoblastic bone destruction in the pelvic transverse plane. (B) (Bone window) Multiple areas of osteoblastic bone destruction in the femoral head transverse plane. (C) (Bone window) Multiple areas of osteoblastic bone destruction in the pelvic coronal plane. (D) (Soft tissue window) The prostate gland demonstrated marked enlargement with calcification.

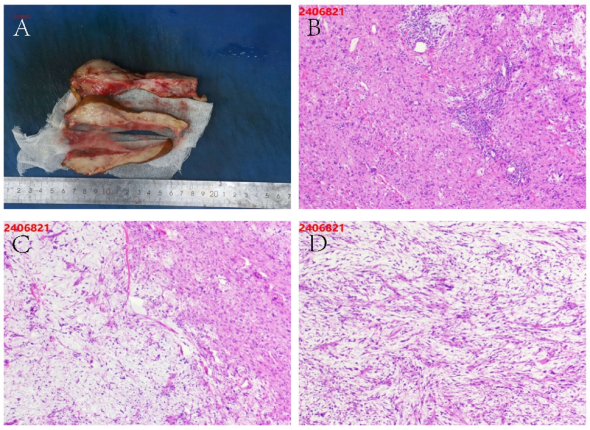

Figure 4. Pathological biopsy of multiple lesions in the left forearm. (A) Gross specimen image of tumor tissue from the left forearm. (B) Tumor cells exhibiting sheet-like growth patterns with lymphocytic infiltration visible in the stroma and perivascular areas. (C) Mucinous degeneration is present in portions of the stroma. (D) Mucinous degeneration is present in portions of the stroma in another section. Hematoxylin and eosin staining; magnification, x100.

After ruling out surgical contraindications, the patient underwent wide excision of the left forearm tumor with skin grafting, vacuum sealing drainage closure and a pubic bone biopsy in April 2024 (Fig. 4A). The operation was successful without obvious postoperative acute complications. The excised tissue was paraffin-embedded after fixation in 4% neutral phosphate-buffered formaldehyde solution at room temperature (~25˚C) for 24 h. Sections were cut at a thickness of

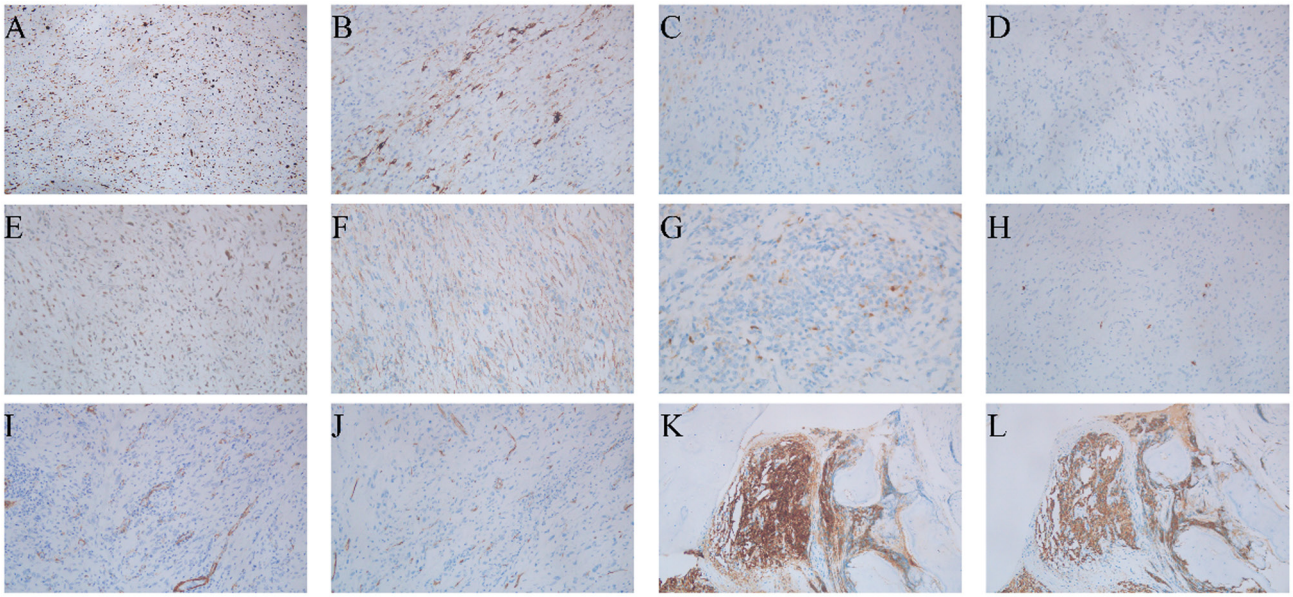

Figure 5. Representative immunohistochemical staining of myxofibrosarcoma and pubic bone metastasis. (A) Ki-67, (B) desmin, (C) p16, (D) p53, (E) MDM2, (F) β-catenin, (G) Pan-tropomyosin receptor kinase, (H) S-100, (I) smooth muscle actin, (J) CD34, (K) prostate-specific antigen, (L) cytokeratin. Magnification, x100.

4 μm and stained with H&E using reagents supplied by Roche Diagnostics (Shanghai) Co., Ltd. at 25˚C for 8 h. The stained slides were examined under a light microscope (Olympus BX43; Olympus Corporation) and representative images were captured for histopathological evaluation. Histopathological analysis of the left forearm tumor demonstrated key features of a high-grade malignant mesenchymal tumor, suggesting a diagnosis of high-grade myxofibrosarcoma (MFS) (4). The tumor was characterized by spindle cells with marked atypia, frequent mitotic figures and multinucleated giant cells, along with myxoid degeneration within the stroma and extensive inflammatory cell infiltration, findings consistent with high-grade MFS (Fig. 4B-D). Additionally, the poorly defined margins, combined with notable cellular pleomorphism, further supported the diagnosis of a highly aggressive malignant mesenchymal tumor.

Immunohistochemical analysis of the left forearm tumor revealed a high proliferative index (Ki-67, 60%) with focal cytoplasmic desmin expression and scattered p16 immunoreactivity (Fig. 5A-C). Tumor cells demonstrated wild-type p53 nuclear expression pattern and weak MDM2 positivity (Fig. 5D and E). β-catenin exhibited preserved membranous localization (Fig. 5F). Notably, pan-tropomyosin receptor kinase (pan-TRK) staining showed weak focal cytoplasmic positivity in 10% of tumor cells without nuclear expression (Fig. 5G). S-100 highlighted scattered interstitial cells, whereas smooth muscle actin (SMA) and CD34 positivity confirmed vascular components (Fig. 5H-J). Finally, the tumor was negative for anaplastic lymphoma kinase (ALK) and SRY-box transcription factor 10 (SOX10), while the reticulin stain demonstrated delicate fibers encircling individual tumor cells (Fig. 6A-C).

The tissue processing and immunohistochemical staining procedures were as follows: Tumor tissues were fixed in 4% neutral phosphate-buffered formaldehyde for 24 h at room temperature (25˚C) and subsequently paraffin-embedded. Paraffin blocks were sectioned into 4-μm slices and baked at 65˚C for 60 min or overnight at 58˚C. Sections were then deparaffinized in three xylene baths (5-10 min each) and rehydrated through a descending alcohol series (100, 95, 85 and 75% each for 2 min). Antigen retrieval and immunostaining were performed using a BenchMark ULTRA automated immunostainer (Roche Diagnostics) at 99˚C for 16 min with an immunohistochemistry antigen retrieval buffer (cat. no. 24005424569188; Roche Diagnostics). Endogenous peroxidase activity was blocked using a peroxidase inhibitor for 5 min at 25˚C. Primary antibodies (prediluted; Roche Diagnostics) were incubated with the sections at 25˚C for 16 min, followed by the OptiView DAB Detection Kit (Roche Diagnostics) according to the manufacturer's protocol. Sections were incubated with OptiView HQ Universal Linker containing horseradish peroxidase (HRP) for 8 min at 25˚C, and subsequently with HRP Multimer for 8 min to visualize staining.

The detailed information on the primary antibodies used in this study is as follows. Ki-67 (Xiamen Talent Biomedical Technology Co., Ltd.; cat. no. AM0241; clone MIB1; 1:200), SMA (Fuzhou Maixin Biotechnology Development Co., Ltd.; cat. no. kit-0006; clone 1A4; 1:100), Desmin [GeneTech (Shanghai) Co., Ltd.; cat. no. GT225229; clone GTM2; 1:300], p16 (Beijing Zhongshan Golden Bridge Biotechnology Co., Ltd.; cat. no. ZM-0205; clone 1C1; 1:300), p53 (Quan Hui Trading International Co., Ltd.; cat. no. AQ20025; clone DO-7; 1:100), MDM2 (Beijing Zhongshan Golden Bridge Biotechnology Co., Ltd.; cat. no. ZM-0425; clone 0TI17B3; ready-to-use), ALK (Beijing Zhongshan Golden Bridge Biotechnology Co., Ltd.; cat. no. TA800712; clone 0TI1H7; ready-to-use), CD34 (Fuzhou Maixin Biotechnology Development Co., Ltd.; cat. no. kit-0004; clone QBEND/10; 1:100), β-Catenin (Beijing Zhongshan Golden Bridge Biotechnology Co., Ltd.; cat.

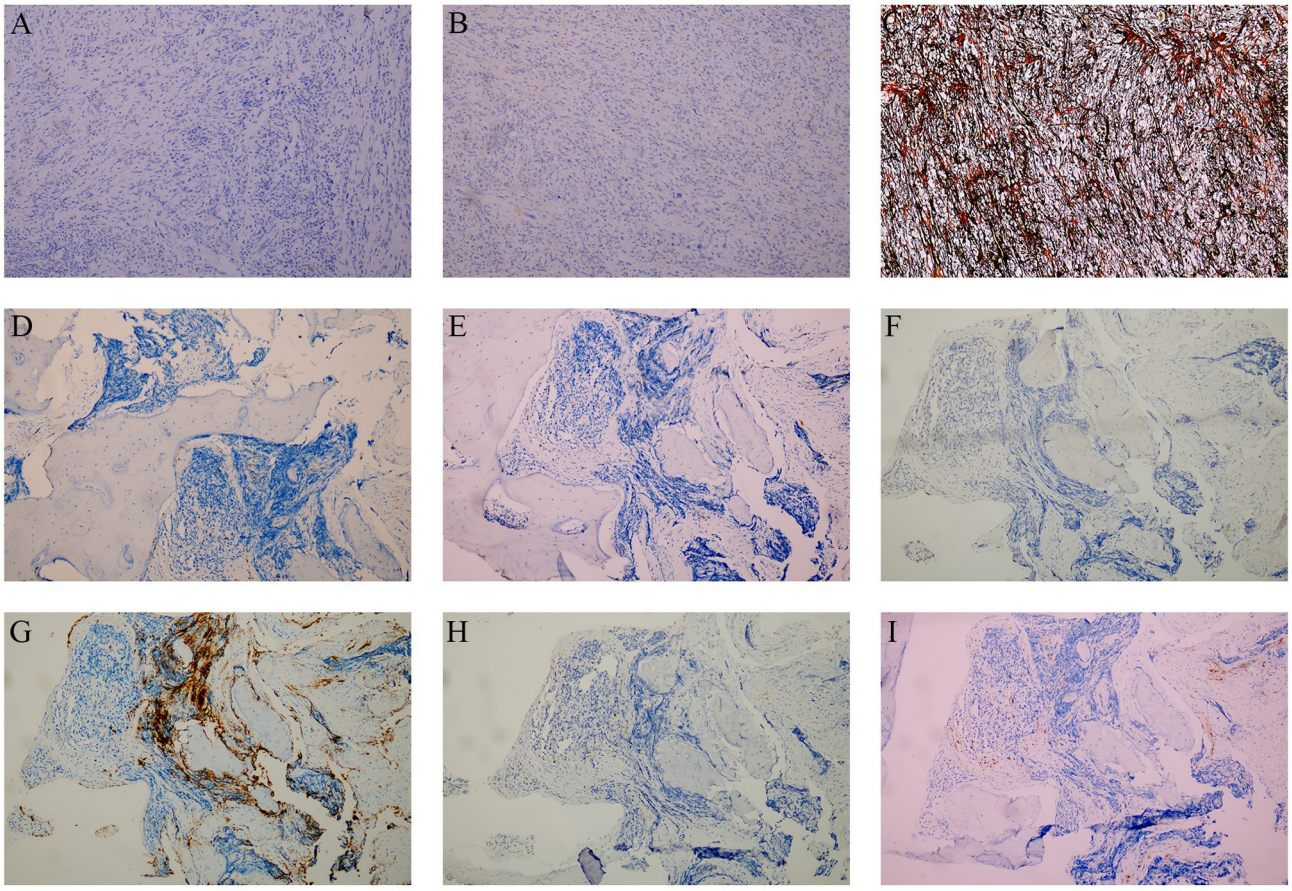

Figure 6. Absence of marker expression in myxofibrosarcoma and pubic symphysis metastasis. (A) Anaplastic lymphoma kinase, (B) SRY-box transcription factor 10, (C) reticulin stain, (D) CD3, (E) CD20, (F) CD61, (G) CD235a, (H) myeloperoxidase and (I) CD38 staining. Magnification, x100.

no. ZM-0442; clone UMAB15; 1:300), pan-TRK (VENTANA Roche; cat. no. 08494665001; clone EPR17341-4; ready-to-use), S-100 (Fuzhou Maixin Biotechnology Development Co., Ltd.; cat. no. kit-0007; clone 4C4.9; 1:100), SOX10 (Xiamen Talent Biomedical Technology Co., Ltd.; cat. no. AM0417; clone SDM2; ready-to-use), PSA (Fuzhou Maixin Biotechnology Development Co., Ltd.; cat. no. MAB-0146; clone ER-PR8; 1:50), CK (Guangzhou Anbiping Pharmaceutical Technology Co., Ltd.; cat. no. IM069; clone AE1&AE3; 1:150), CD3 (Quan Hui Trading International Co., Ltd.; cat. no. NCL-L-CD3-565; clone LN10; 1:50), CD20 (Fuzhou Maixin Biotechnology Development Co., Ltd.; cat. no. kit-0001; clone L26; 1:1), CD61 (Agilent Technologies Singapore International; cat. no. 8930248; clone VI-PL2; 1:100), CD235a (Fuzhou Maixin Biotechnology Development Co., Ltd.; cat. no. MAB-0603; clone JC159; ready-to-use), MPO (Quan Hui Trading International Co., Ltd.; cat. no. AQ20285; polyclonal; 1:100) and CD38 (Quan Hui Trading International Co., Ltd.; cat. no. NCL-L-CD38-290; clone SPC32; 1:100).

Reticulin staining was performed on formalin-fixed paraffin-embedded sections using standard protocols. Slides were counterstained with hematoxylin for 8 min and eosin for 1 min at room temperature and examined under a light microscope (Olympus BX53) at x100 magnification.

Subsequently, histopathological analysis of the pubic bone biopsy confirmed metastatic prostate cancer. Gross examination revealed multiple gray-white specimens from the pubic bone (Fig. 7A). Microscopically, the fibrous tissue surrounding the lesion exhibited marked proliferation and infiltrative growth of epithelioid cells, characterized by abundant cytoplasm, prominent nucleoli and pleomorphic features, consistent with metastatic adenocarcinoma of prostatic origin (Fig. 7B and C). Immunohistochemistry further demonstrated PSA and cytokeratin positivity (Fig. 5K and L), while hematopoietic markers (CD3, CD20 and MPO), megakaryocytic/erythroid markers (CD61 and CD235a) and the plasma cell marker (CD38) were uniformly negative (Fig. 6D-I). These findings, in conjunction with the notably elevated serum PSA levels and the clinical profile, conclusively supported a diagnosis of advanced metastatic prostate cancer. Given the unequivocal histopathological confirmation of osseous metastasis in this octogenarian patient, a prostate biopsy was deemed unwarranted per multidisciplinary consensus guidelines.

Postoperatively, the patient was treated with cefuroxime sodium (1.5 g twice daily, i.v.), papaverine hydrochloride (30 mg i.v.), celecoxib (0.2 g twice daily, p.o.) and rabeprazole sodium (10 mg p.o.) for anti-infection, circulation improvement, analgesia, and gastric protection, respectively. The patient demonstrated favorable recovery and remained in stable condition, with no other notable concurrent interventions. The patient exhibited good treatment compliance and reported no significant discomfort. By August 2024, the patient had achieved a marked recovery, maintained a stable appetite and regular sleep patterns, adhered to scheduled

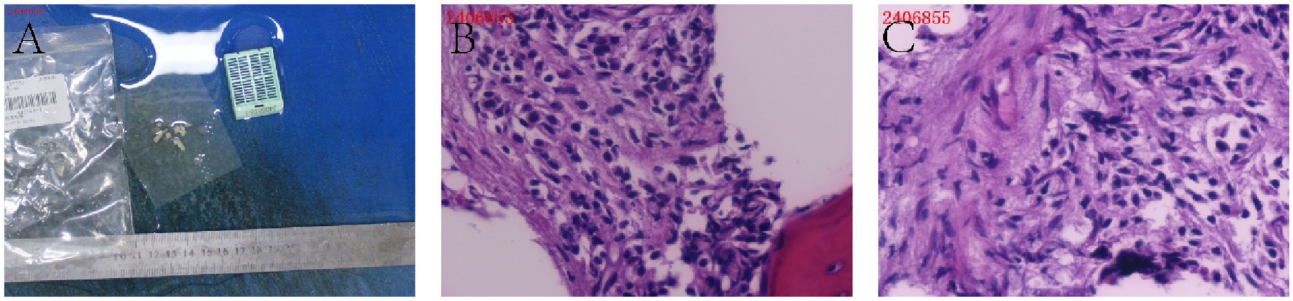

Figure 7. Pathological biopsy of the pubic bone. (A) Multiple gray-white gross specimens from the pubic bone. (B) Anisomorphic epithelial-like cells (cancer cells) with infiltrative growth are visible in the fibrous tissue. (C) Another section demonstrates cellular atypical growth. Hematoxylin and eosin staining; magnification, x200.

follow-up visits and continued a routine regimen of bone pain medication. As of September 2025, the patient remained alive, in stable condition and under regular follow-up. The final diagnosis of metachronous multiple primary malignant neoplasms (MMPMNs; high-grade myxofibrosarcoma of the left forearm and prostate adenocarcinoma with osseous metastasis) was thus established.

Discussion

MFS, formerly classified as a subtype of malignant fibrous histiocytoma, predominantly affects patients aged 40 to 80 years (8,9). In total, two-thirds of MFS cases arise in superficial soft tissues, typically the deep dermis and subcutis of the limbs, while the remainder occur in deeper subfascial or intramuscular locations (9,10). Histologically, MFS is distinguished by a myxoid extracellular matrix, pleomorphic spindle cells and characteristic curvilinear blood vessels (11). Patients with MFS exhibit a notably elevated risk of developing subsequent primary malignancies (12). Following the analysis of a retrospective cohort, Tateishi *et al* (13) reported 5- and 10-year cumulative incidences of secondary cancers of 16.9%, significantly exceeding rates seen in other sarcoma subtypes (hazard ratio, 2.34; 95% confidence interval, 1.01-5.41; P=0.048). In that cohort, patients with MFS who developed secondary malignancies exhibited a wide spectrum of additional tumor types involving multiple organ systems. The secondary cancers most frequently comprised adenocarcinomas arising in the stomach, ovary, prostate, colon, cecum, breast, kidney, lung and rectum. Other histological subtypes included squamous cell carcinomas of the pharynx, tongue, gingiva and esophagus, as well as transitional cell carcinoma of the bladder and renal cell carcinoma of the kidney. These neoplasms represented independent primary tumors coexisting with MFS rather than metastatic lesions, with some diagnosed prior to and others following the onset of sarcoma. This series also included a case of metachronous prostate adenocarcinoma following MFS, mirroring the observation of occult prostate cancer detected via superscan in the present study.

Beyond the risk of additional primary tumors, MFS poses its own clinical challenges due to aggressive behavior and high local recurrence rates, particularly in high-grade tumors. Recurrence rates for MFS rank among the highest of all soft-tissue sarcomas, underscoring the necessity for rigorous surveillance (14,15). Although distant metastases are less frequent (occurring in 13-16% of cases), the lungs and brain are the most common sites, with occasional spread to the small intestine, pelvis, retroperitoneum, stomach, liver and adrenal glands (16,17). In the present study, the paradoxical finding of a superscan (indicating diffuse osteoblastic activity) combined with intact cortical bone adjacent to the sarcoma and the rarity of MFS metastasis to prostate or bone strongly supports the diagnosis of multiple primary malignancies rather than metastatic spread.

Following intravenous administration of ^{99m}Tc-MDP, nuclear imaging techniques such as SPECT and positron emission tomography (PET) assess the skeletal biodistribution of the tracer, mediated by its affinity for hydroxyapatite in bone tissue. While physiological uptake in soft tissues may occasionally occur, abnormal extraosseous radiotracer accumulation warrants further investigation. Research highlights a strong correlation between radiotracer deposition and malignancies, primarily driven by metastatic spread or primary soft-tissue tumors, reflecting its critical diagnostic application in oncological settings (18-20). Soft-tissue tumors in the limbs are frequently characterized by increased blood volume within malignant tissues, driven by tumor-induced angiogenesis. As a result, this vascular proliferation leads to abnormal tracer accumulation as the enhanced and permeable vasculature facilitates tracer retention in non-target regions, complicating the accuracy of imaging interpretation (21).

A superscan represents a distinctive pattern observed in three-phase bone imaging, characterized by diffuse and intense skeletal uptake, and accompanied by markedly diminished soft tissue and renal activity. While, under normal conditions, the tracer uptake ratio between the skeletal system and kidneys is ~2:3, in cases of a superscan, this ratio may shift to as high as 17:3 (22), indicating significant deviations from typical tracer distribution. Given the inherent complexities involved in achieving objective quantification, the accurate diagnosis of a superscan is particularly challenging and often necessitates the specialized expertise and interpretive skills of experienced nuclear medicine physicians (23). Superscan is frequently associated with conditions that promote diffuse reactive bone formation, such as bone metastases from malignancies and certain metabolic bone diseases (24,25). Notably, this phenomenon has been documented in the literature as an unexpected indicator of occult prostate cancer, underscoring the critical role of bone scintigraphy as a diagnostic alert for asymptomatic secondary malignancies (26). Data indicate that

superscan occurs in 15-23% of patients with prostate cancer, establishing the disease as the most common underlying cause. Although other malignancies, including gastric and breast cancer, are also capable of inducing superscan, their incidence remains significantly lower by comparison (25). Given the broad differential diagnosis associated with superscan, visual interpretation alone is insufficient. Laboratory tests (such as serum calcium and alkaline phosphatase), tumor markers and additional imaging are critical for an accurate diagnosis.

In the present study, X-ray, thin-section bone-window CT and 3D-CT were not performed for the patient due to financial constraints and comorbidities, which limits the anatomical assessment and the exclusion of microscopic bone invasion. Future similar cases should incorporate these imaging modalities to enhance lesion characterization and diagnostic precision.

Although the present case lacked molecular profiling, available data indicate key genetic alterations in both malignancies (MFS and prostate cancer) that may reveal shared oncogenic pathways. MFS often harbors TP53 mutations and CDKN2A deletions, leading to disrupted cell-cycle control and genomic instability, while prostate adenocarcinoma frequently features androgen receptor amplification and PTEN loss, driving tumor growth and metastatic potential (27,28). Furthermore, prostate-specific membrane antigen (PSMA; classically upregulated in prostate cancer) is also detected in the neovasculature of sarcomas (up to 35.3% in MFS), where it promotes angiogenesis and may contribute to increased ^{99m}Tc-MDP uptake in a superscan (29,30). Both tumor types express luteinizing hormone-releasing hormone (LHRH) receptors, suggesting potential benefit from LHRH-targeted therapies (31). Emerging evidence implicates dysregulated p53 signaling, PI3K/AKT pathway activation and an immunosuppressive tumor microenvironment characterized by tumor-associated macrophage infiltration and T-cell exhaustion as possible common mechanisms underlying multiple primary malignancies (32-34). Future studies should employ comprehensive genomic sequencing and immune profiling to identify overlapping driver mutations, clarify the role of PSMA-mediated angiogenesis and LHRH pathways, and evaluate whether targeted or immunomodulatory treatments can mitigate the risk of metachronous tumors.

MPMNs within the same individual are identified by the presence of distinct pathological features in each tumor (1-4). Traditionally, the diagnosis of MPMN is based on the Warren criteria (35) and revisions by Liu *et al* (36). However, the Surveillance, Epidemiology and End Results (SEER) and International Agency for Research on Cancer/International Association of Cancer Registries (IARC/IACR) guidelines have become integral to modern diagnostics, serving to enhance and extend the criteria used for diagnosing MPMNs. SEER emphasizes tumor histology, anatomical location, laterality and the time interval between diagnoses, thereby facilitating the identification of multiple independent primary tumors (37). By contrast, the IARC/IACR criteria are more conservative, typically registering only one tumor per organ or paired organs, emphasizing histological consistency and adopting a cautious approach to multiple tumors in the same anatomical site (38).

Synchronous MPMNs (SMPMNs) are defined as two or more primary malignancies diagnosed within 6 months, while those diagnosed after 6 months are termed metachronous MPMNs (MMPMNs). MMPMNs have a lower incidence but similar survival rate compared with SMPMNs (3,5). In the present case, the patient was diagnosed with MMPMNs, comprising high-grade myxofibrosarcoma of the left forearm and prostate adenocarcinoma with osseous metastasis, as the two malignancies were identified more than 6 months apart. Tumor growth patterns, treatment approaches and individual variability can affect the timing of diagnosis. Data suggest a median interval of 3.45-6.13 years between the diagnoses of the first and second primary tumors in MMPMN, but the prognostic relevance of this interval remains uncertain (5,6,39). Regardless, early detection, precise diagnosis and prompt treatment are critical to improving outcomes in MPMNs. While imaging techniques such as SPECT/CT and PET/CT enhance diagnostic accuracy, pathological examination remains the gold standard when MPMN cannot be ruled out.

In the evaluation of MFS, ^{18}F-fluorodeoxyglucose (^{18}F-FDG) PET/CT can offer valuable metabolic information, while ^{99m}Tc-MDP three-phase bone scintigraphy is traditionally used to detect osteoblastic activity and assess potential bone metastases, often demonstrating only minimal soft-tissue uptake (40). Although in the present study bone scintigraphy revealed increased perfusion and focal ^{99m}Tc-MDP accumulation in the left forearm, suggestive of soft-tissue malignancy, and produced a classic superscan pattern indicative of diffuse skeletal involvement, it lacks the specificity to distinguish primary sarcoma from metastatic disease. By contrast, ^{18}F-FDG PET/CT quantifies tumor glucose metabolism, achieving sensitivity rates of >90% for soft-tissue sarcomas compared with ~70% for planar bone scans, and can detect microscopic cortical or marrow invasion that may be occult on bone scintigraphy or MRI (41,42). In the present study, ^{18}F-FDG PET/CT was not performed due to the advanced age, frailty and financial constraints of the patient, which constitutes a limitation of the diagnostic workup. While ^{99m}Tc-MDP SPECT/CT has high utility for detecting widespread bone metastatic activity (superscan), its sensitivity (~86.7%) and specificity (~98.8%) for prostate cancer bone metastases are slightly inferior to those of ^{18F}fluorocholine PET/CT, which achieves a sensitivity of up to 93.3% and a specificity of 100% in biochemical recurrence settings (43,44). A prospective comparative study also showed that NaF PET/CT attains a sensitivity of ~95% and a specificity of ~93%, marginally outperforming SPECT/CT and MRI (45). Moreover, ^{18}F-DCFPyL PET/CT demonstrated superior diagnostic accuracy vs. ^{99m}Tc-MDP SPECT/CT in a direct head-to-head study (46). Together, these findings indicate that PET/CT modalities, especially PSMA-targeted or choline-based tracers and NaF PET, offer significantly higher sensitivity and specificity compared with conventional bone SPECT/CT in prostate cancer bone metastasis detection.

In the present study, preserved cortical bone integrity was confirmed via histopathological microsectioning, effectively ruling out local invasion despite the presence of a superscan pattern. Given this discordance, PSA testing (563.864 ng/ml) and hip CT were pursued, which, combined with SPECT/CT fusion imaging, identified prostate enlargement and mixed sclerotic/lytic lesions consistent with metastatic prostate cancer. The final diagnosis of metachronous MPMN (high-grade MFS and prostate adenocarcinoma) was thus established.

Nonetheless, the absence of PET/CT imaging and molecular profiling remains a limitation, and we recommend employing PET/CT or CT bone-window imaging in similar future cases to enhance diagnostic accuracy and to better distinguish primary soft-tissue tumors from skeletal metastases.

In conclusion, the present study describes a rare case involving dual primary malignancies (subcutaneous MFS and prostate cancer with extensive bone metastases) diagnosed through ^{99m}Tc-MDP three-phase bone scintigraphy. The unique imaging characteristics, specifically the extensive metastases on superscan bone imaging and its established association with occult prostate cancer, together with the patterns of recurrence and metastasis of the primary tumor, were pivotal in informing and shaping the subsequent therapeutic approach. Given the scarce reports of MPMNs identified through ^{99m}Tc-MDP scintigraphy, the present case highlights the need for heightened clinical vigilance. For patients with recurrent soft-tissue sarcoma who demonstrate a superscan on bone scintigraphy, routine screening for occult prostate carcinoma should be undertaken. For any patient newly diagnosed with a malignancy, clinicians should integrate detailed clinical evaluation with three-phase bone imaging findings to eliminate suspicion for additional primary tumors. Such a strategy enhances diagnostic precision, reduces the likelihood of missed or incorrect diagnoses and facilitates individualized treatment planning that may improve overall patient outcomes.

Acknowledgements

Not applicable.

Funding

No funding was received.

Availability of data and materials

The data generated in the present study may be requested from the corresponding author.

Authors' contributions

JYL, JLL, HYZ, SXY and JSZ confirm the authenticity of all the raw data. JYL, JLL, HYZ and JSZ contributed to the conception of the study. JYL, JLL and SXY were responsible for writing the original draft and reviewing and editing the manuscript. SXY was responsible for the acquisition of clinical data. JSZ was responsible for critical revision of the manuscript and the analysis and interpretation of the data. All authors have read and approved the final version of the manuscript.

Ethics approval and consent to participate

This study passed ethical review by the Ethics Committee of the Third Affiliated Hospital of Guangzhou Medical University (Guangzhou, China). No information that could potentially compromise patient privacy or personal identity was included in this article. All the data used in this study were collected from the Third Affiliated Hospital of Guangzhou Medical University with both written and verbal informed consent from the patient.

Patient consent for publication

All the test results, images and permission for their publication were obtained with written consent from the patient.

Competing interests

The authors declare that they have no competing interests.

References

1. Warren S and Gates O: Multiple primary malignant tumors. A survey of the literature and stasistical study. Am J Cancer 16: 1358-1414, 1932.
2. Liu F, Qin D and Wang Q: Clinical pathological analysis of 172 cases with multiple primary carcinoma. Chin J Oncol 1: 113-119, 1979.
3. Moertel CG, Dockerty MB and Baggenstoss AH: Multiple primary malignant neoplasms. I. Introduction and presentation of data. Cancer 14: 221-230, 1961.
4. Shi L, Zhou S, Jiang Y, Wan Y, Ma J, Fu S and Cheng W: Gynecological malignant tumor related multiple primary malignant neoplasms: Clinical analysis of 30 cases. Zhonghua Fu Chan Ke Za Zhi 49: 199-203, 2014.
5. Xu LL and Gu KS: Clinical retrospective analysis of cases with multiple primary malignant neoplasms. Genet Mol Res 13: 9271-9284, 2014.
6. Wang Y, Jiao F, Yao J, Zhou X, Zhang X and Wang L: Clinical features of multiple primary malignant tumors: A retrospective clinical analysis of 213 Chinese patients at two centers. Discov Med 32: 65-78, 2021.
7. Vogt A, Schmid S, Heinimann K, Frick H, Herrmann C, Cerny T and Omlin A: Multiple primary tumours: Challenges and approaches, a review. ESMO Open 2: e000172, 2017.
8. Pauli C, De Boni L, Pauwels JE, Chen Y, Planas-Paz L, Shaw R, Emerling BM, Grandori C, Hopkins BD and Rubin MA: A functional precision oncology approach to identify treatment strategies for myxofibrosarcoma patients. Mol Cancer Res 20: 244-252, 2022.
9. Rachdi I, Daoud F, Khanchel F, Arbaoui I, Somai M, Zoubeidi H, Aydi Z, Ben Dhaou B, Debbiche A and Boussema F: Myxofibrosarcoma of the leg: A diagnostic challenge. Clin Case Rep 8: 3332-3335, 2020.
10. Zhang P, Ruan SF, Huang J, Gong T and Ji C: Multiple cutaneous myxofibrosarcoma on the right arm: Clinicopathological features and differential diagnosis. Authorea, 2023.
11. Vanni S, De Vita A, Gurrieri L, Fausti V, Miserocchi G, Spadazzi C, Liverani C, Cocchi C, Calabrese C, Bongiovanni A, *et al*: Myxofibrosarcoma landscape: Diagnostic pitfalls, clinical management and future perspectives. Ther Adv Med Oncol 14: 17588359221093973, 2022.
12. Fernebro J, Bladström A, Rydholm A, Gustafson P, Olsson H, Engellau J and Nilbert M: Increased risk of malignancies in a population-based study of 818 soft-tissue sarcoma patients. Br J Cancer 95: 986-990, 2006.
13. Tateishi U, Hasegawa T, Yamamoto S, Yamaguchi U, Yokoyama R, Kawamoto H, Satake M and Arai Y: Incidence of multiple primary malignancies in a cohort of adult patients with soft tissue sarcoma. Jpn J Clin Oncol 35: 444-452, 2005.
14. Sanfilippo R, Miceli R, Grosso F, Fiore M, Puma E, Pennacchioli E, Barisella M, Sangalli C, Mariani L, Casali PG and Gronchi A: Myxofibrosarcoma: Prognostic factors and survival in a series of patients treated at a single institution. Ann Surg Oncol 18: 720-725, 2011.
15. Mentzel T, Calonje E, Wadden C, Camplejohn RS, Beham A, Smith MA and Fletcher CD: Myxofibrosarcoma. Clinicopathologic analysis of 75 cases with emphasis on the low-grade variant. Am J Surg Pathol 20: 391-405, 1996.
16. Neagu TP, Sinescu RD, Enache V, Achim SC, Ţigliş M and Mirea LE: Metastatic high-grade myxofibrosarcoma: Review of a clinical case. Rom J Morphol Embryol 58: 603-609, 2017.
17. Look Hong NJ, Hornicek FJ, Raskin KA, Yoon SS, Szymonifka J, Yeap B, Chen YL, DeLaney TF, Nielsen GP and Mullen JT: Prognostic factors and outcomes of patients with myxofibrosarcoma. Ann Surg Oncol 20: 80-86, 2013.
18. Castaigne C, Martin P and Blocklet D: Lung, gastric, and soft tissue uptake of Tc-99m MDP and Ga-67 citrate associated with hypercalcemia. Clin Nucl Med 28: 467-471, 2003.

19. Flores LGI, Nagamachi S, Jinnouchi S, Ohnishi T, Futami S, Nakahara H and Tamura S: Relationship between extraosseous accumulation in bone scintigraphy with 99Tcm-HMDP and histopathology. Nucl Med Commun 19: 347-354, 1998.
20. Zeng D, Chen Y, Cai L and Zhou F: Analysis of abnormal uptake of extraskeletal soft tissue in ^{99m}Tc-MDP whole bone scan. Chongqing Med J 45: 2073-2077, 2016 (In Chinese).
21. Ostergaard L, Tietze A, Nielsen T, Drasbek KR, Mouridsen K, Jespersen SN and Horsman MR: The relationship between tumor blood flow, angiogenesis, tumor hypoxia, and aerobic glycolysis. Cancer Res 73: 5618-5624, 2013.
22. Buckley O, O'Keeffe S, Geoghegan T, Lyburn ID, Munk PL, Worsley D and Torreggiani WC: 99mTc bone scintigraphy superscans: A review. Nucl Med Commun 28: 521-527, 2007.
23. Ren JYL, Li Y and Luo Y: Differentiation of superscan in ^{99}TC^{m}-MDP bone scintigraphy: A case report. Chin J Nucl Med Mol Imaging 39: 39-40, 2019 (In Chinese).
24. Askari E, Shakeri S, Roustaei H, Fotouhi M, Sadeghi R, Harsini S and Vali R: Superscan pattern on bone scintigraphy: A comprehensive review. Diagnostics (Basel) 14: 2229, 2024.
25. Kovacsne A, Kozon I, Bentestuen M and Zacho HD: Frequency of superscan on bone scintigraphy: A systematic review. Clin Physiol Funct Imaging 43: 297-304, 2023.
26. Prakash R: Incidental detection of skeletal metastases on technetium-99m DTPA renal scintigraphy. Australas Radiol 39: 182-184, 1995.
27. Ogura K, Hosoda F, Arai Y, Nakamura H, Hama N, Totoki Y, Yoshida A, Nagai M, Kato M, Arakawa E, *et al*: Integrated genetic and epigenetic analysis of myxofibrosarcoma. Nat Commun 9: 2765, 2018.
28. Bui NQ, Przybyl J, Trabucco SE, Frampton G, Hastie T, van de Rijn M and Ganjoo KN: A clinico-genomic analysis of soft tissue sarcoma patients reveals CDKN2A deletion as a biomarker for poor prognosis. Clin Sarcoma Res 9: 12, 2019.
29. Kleiburg F, van der Hulle T, Gelderblom H, Slingerland M, Speetjens FM, Hawinkels LJAC, Dibbets-Schneider P, van Velden FHP, Pool M, Lam SW, *et al*: PSMA expression and PSMA PET/CT imaging in metastatic soft tissue sarcoma patients, results of a prospective study. Eur J Nucl Med Mol Imaging 52: 3690-3699, 2025.
30. Spiridon IA, Ong SLM, Soukup J, Topirceanu-Andreoiu OM, de Geus-Oei LF, Gelderblom H, Lam SW, de Bruijn IHB, Akker BEWMVD, Hijmen L, *et al*: Neovascular prostate specific membrane antigen (PSMA) expression in bone and soft tissue sarcoma: A systematic analysis. Virchows Arch: Apr 9, 2025 (Epub ahead of print).
31. Deivaraju C, Temple HT, Block N, Robinson P and Schally AV: LHRH receptor expression in sarcomas of bone and soft tissue. Horm Mol Biol Clin Investig 28: 105-111, 2016.
32. Wu H, Li J, Yao R, Liu J, Su L and You W: Focusing on the interplay between tumor-associated macrophages and tumor microenvironment: from mechanism to intervention. Theranostics 15: 7378-7408, 2025.
33. Zhang Z and Wu Y: Research progress on mechanisms of tumor immune microenvironment and gastrointestinal resistance to immunotherapy: Mini review. Front Immunol 16: 1641518, 2025.
34. Nair R, Somasundaram V, Kuriakose A, Krishn SR, Raben D, Salazar R and Nair P: Deciphering T-cell exhaustion in the tumor microenvironment: Paving the way for innovative solid tumor therapies. Front Immunol 16: 1548234, 2025.
35. Swaroop VS, Winawer SJ, Kurtz RC and Lipkin M: Multiple primary malignant tumors. Gastroenterology 93: 779-783, 1987.
36. Liu F, Qin D and Wang Q: Clinical and pathological analysis of 172 cases of multiple primary cancers. Chin J Oncol 1: 113-119, 1979 (In Chinese).
37. Adamo M, Johnson C, Ruhl J and Dicki L (eds): SEER program coding and staging manual. NIH publication number 12-5581. National Cancer Institute, Bethesda, MD, 2012.
38. Working Group Report: International rules for multiple primary cancers (ICD-0 third edition). Eur J Cancer Prev 14: 307-308, 2005.
39. Tichansky DS, Cagir B, Borrazzo E, Topham A, Palazzo J, Weaver EJ, Lange A and Fry RD: Risk of second cancers in patients with colorectal carcinoids. Dis Colon Rectum 45: 91-97, 2002.
40. Ito K, Masuda-Miyata Y, Wada S, Morooka M, Yamasawa K, Hashimoto M and Kubota K: F-18 FDG PET/CT imaging of bulky myxofibrosarcoma in chest wall. Clin Nucl Med 36: 212-213, 2011.
41. Younis MH, Abu-Hijleh HA, Aldahamsheh OO, Abualruz A and Thalib L: Meta-analysis of the diagnostic accuracy of primary bone and soft tissue sarcomas by 18F-FDG-PET. Med Princ Pract 29: 465-472, 2020.
42. Kassem TW, Abdelaziz O and Emad-Eldin S: Diagnostic value of ^{18}F-FDG-PET/CT for the follow-up and restaging of soft tissue sarcomas in adults. Diagn Interv Imaging 98: 693-698, 2017.
43. Shen G, Deng H, Hu S and Jia Z: Comparison of choline-PET/CT, MRI, SPECT, and bone scintigraphy in the diagnosis of bone metastases in patients with prostate cancer: A meta-analysis. Skeletal Radiol 43: 1503-1513, 2014.
44. de Leiris N, Leenhardt J, Boussat B, Montemagno C, Seiller A, Phan Sy O, Roux J, Laramas M, Verry C, Iriart C, *et al*: Does whole-body bone SPECT/CT provide additional diagnostic information over [18F]-FCH PET/CT for the detection of bone metastases in the setting of prostate cancer biochemical recurrence? Cancer Imaging 20: 58, 2020.
45. Zamani-Siahkali N, Mirshahvalad SA, Farbod A, Divband G, Pirich C, Veit-Haibach P, Cook G and Beheshti M: SPECT/CT, PET/CT, and PET/MRI for response assessment of bone metastases. Semin Nucl Med 54: 356-370, 2024.
46. Hu X, Cao Y, Ji B, Zhao M, Wen Q and Chen B: Comparative study of ^{18}F-DCFPyL PET/CT and ^{99m}Tc-MDP SPECT/CT bone imaging for the detection of bone metastases in prostate cancer. Front Med (Lausanne) 10: 1201977, 2023.